Circuits, Systems, and Signal Processing (2022) 41:6885–6905
https://doi.org/10.1007/s00034-022-02084-6

A Novel Denoising Method for Medical CT Images Based on Moving Decomposition Framework

Ju Zhang[1] · JinCheng Lv[2] · Yun Cheng[3]

Received: 26 November 2021 / Revised: 6 June 2022 / Accepted: 6 June 2022 /
Published online: 19 July 2022

Abstract

In the past decades, CT images have been widely used and played a critical role in medical diagnosis. However, low-dose CT images are often contaminated by noise, this being the most important factor affecting the quality of a CT image. This paper proposes a novel integrated framework and a denoising method for low-dose medical CT images to obtain a better denoising effect whilst at the same time preserving an image's local structure information. First, an image moving decomposition is employed to decompose the CT image. The original CT noisy image is decomposed, and the components will be processed separately, so that the details and edges of the CT image can be better preserved. Next, the Shearlet Transformation-based denoising method is applied to the component which contains edges and detailed information of the CT image. The multi-directionality and multi-scale property of the Shearlet make it possible to obtain better effect in denoising the detail parts. BM3D filtering is used to remove noise in the component similar to the origin image, and obtain ideal denoising results in denoising the approximate components (mainly low frequency part) of the CT image. With the two processed components and the inverse decomposition, the denoised image is obtained. Finally, simulations and clinical experiments are conducted and comparisons made. The experimental results show the proposed denoising method can obtain better performances in terms of PSNR value, SSIM and FoM and

✉ Yun Cheng
962110508@qq.com

Ju Zhang
juzhang@hznu.edu.cn

JinCheng Lv
463745696@qq.com

1 College of Information Science and Technology, Hangzhou Normal University, Hangzhou, China

2 College of Information Engineering, Zhejiang University of Technology, Hangzhou, China

3 Department of Ultrasound, Zhejiang Hospital, Hangzhou, China

thus have very competitive results compared with other existing CT denoising methods.

Keywords Medical CT imaging · Shearlet transformation · Moving decomposition framework · BM3D

1 Introduction

Compared with conventional X-ray techniques and their deficiency in being unable to distinguish muscles, ligaments, blood vessels and other organs, computed tomography (CT) techniques make medical imaging more precise thus much more effective. The cross section image obtained by CT has high density resolution, accuracy in thickness, is clear and without interference from the structure outside the plane. However, the extensive uses of CT in medical practice have raised a public concern over the associated radiation dose to patients [7]. Reducing the radiation dose may lead to increased noise and artifacts, which can adversely affect the radiologists' judgment and confidence [11]. Hence, extensive efforts have been made in recent years to develop better image reconstruction or image processing methods to reduce low-dose CT noise and suppress artifacts.

The denoising methods, proposed in the literatures, are in fact to mainly denoise the low-dose CT image. In recent years, many researchers have proposed new denoising methods. There are spatial domain filters like the Wiener filter [19], which calculates the local mean and variance of the image. The pixel value of a point in the image is calculated according to the estimation of local variance. The Wiener filter has a better suppression effect on Gaussian noise than median filter. However, Wiener filtering often reduces the edge information of the image while suppressing the noise.

The non-local means (NLM) filter, proposed by Buades, works on the basis that adjacent pixels have some kind of correlations and these can be expressed as the values of their weights. The NLM filter replaces the target pixel value by the weighted sum of the pixel values in the window on an image, the closer to the target pixel, the greater the weight of one certain pixel in the window [2]. NLM filtering considers the self-similarity of pixels in the image. It can identify better than traditional bilateral filtering the details of the image as NLM determines the similarity of the two pixels according to the similarity between the images with a certain size. Li et al. [15] proposed a NLM-based CT denoising algorithm, which improves the traditional NLM algorithm by addressing the fact that uniform filtering strength in NLM cannot deal with a situation where the noise level of each slice of CT image is different. In the literature [16], an adapted denoising algorithm for CT image using NLM is proposed. By integrating NLM with correlation-based wavelet packet thresholding, a CT image denoising method is proposed in the literature [8], which can improve the detail preserve ability compared with that using NLM. However, the time cost of NLM filtering is seriously affected by image size and search window size. As the size of the image or the size of the search window increases, the time required for denoising increases rapidly, and the size of the search window often determines the denoising performances of the NLM filter.

Having a similar but improved process on image denoising, block matching 3D denoising (BM3D) was proposed [5]. BM3D combines the strategy of block-wise estimation and transformation domain filtering, and thus it is a kind of hybrid domain filter. In the stage of block-wise estimation, the image will go through the process of block matching, and the BM3D algorithm makes full use of the redundancy of the 3D image block groups. This comes from the process of block matching by filtering these block groups with a 3D sparse transformation-based denoising algorithm, and thus BM3D is faster and more efficient than NLM. The PSNR value of the image with BM3D denoising is excellent.

Shearlets, a typical method of transformation domain filter has been extensively studied and can obtain both the location and direction information of the signal [6, 13, 17, 22]. Shearlets have optimal sparse approximation properties in combination with their unified treatment of the continuum and digital realm. Wavelet transformation has become a powerful tool for signal analysis in recent decades. Wavelets are optimally efficient in representing functions with point-wise singularities. However, Wavelets are very limited at catching the regularity of edge curves because Wavelets cannot provide a sparse representation for line or curve singularities. Compared with Wavelets, the multi-directional frequency-domain support of Shearlets makes the Shearlet more sensitive to the capture of the singular curve and more sensitive to anisotropy features.

G. Ghimpeteanu et al. proposed a new method to provide a Moving Decomposition Framework (MDF) to the denoising process [9]. The basis of this method is to compute the components of the image in a moving frame that encodes its local geometry (directions of gradients and level lines). Processing of these components is more effective than processing directly on the origin images. Three different denoising methods are reported to have been improved with the MDF, i.e. a local variational method, a patch-based method, and a method combining the patch-based with a filtering in spectral domain approach.

The K-SVD method is usually used for image denoising, and its effect is very remarkable. The K-SVD method realizes denoising by sparse coding. The noisy image can be regarded as composed of the original image and noise. The original image is considered sparse, that is, can be represented by a finite number of atoms, while the noise is random and non-sparse. Therefore, sparse components can be extracted and then used to reconstruct the image. In this process, the noise is discarded as the residual between the observation image and the reconstructed image, thus playing a role of noise reduction. Inspired by compressed sensing methods, an adapted K-SVD method was proposed [4] to reduce artifacts in CT images.

The recent explosive development of deep neural networks suggests new thinking and huge potential for the medical imaging field, and deep learning is introduced in the denoising methods for CT image [3, 18, 20]. In the literature [21], a low-dose CT image denoising method using generative adversarial network with Wasserstein distance and perceptual loss is proposed. The residual network, while increasing the number of network layers, can also guarantee the performance of the neural network, and has a good improvement on the training problems such as overfitting. In the image denoising convolutional neural network (DnCNN), the residual learning method is used to learn and train the image noise to obtain an image denoising model [23, 24]. A CNN and multi-feature extraction-based denoising method with a combination of

batch normalization and residual learning is proposed to solve the problem of noise removal in medical CT images [25]. Because of the black box nature of deep learning-based method, the dependence on neural network structure model and training data set, deep learning-based denoising methods usually make it difficult to obtain stable results in CT image denoising.

The contributions of the proposed method are as follows:

- A novel integrated framework and denoising method for medical CT images was proposed to obtain better denoising results, so that CT image denoising must reduce the image noise while retaining the details and edges of the CT image.
- The noisy CT image is decomposed and the components are processed separately. Different denoising methods are utilized to deal with the high frequency band and low frequency band respectively, so that the details and edges of the CT image can be better preserved.
- The multi-directionality and multi-scale property of the Shearlets enable to obtain better effect in denoising the detail parts, and the BM3D obtain ideal denoising results in denoising the approximate components.
- Simulations and clinical experiments are conducted and comparisons made with other existing methods, showing the proposed denoising method can obtain better performances in terms of PSNR value, SSIM and FoM.

The organization of this paper is as follows. Section 2 presents the main idea of the proposed algorithm and the schematic diagram of the proposed method. The main constructing components of the approach are also illustrated in this section. Section 3 presents the experimental and comparison studies of the proposed approach. Conclusions and some perspectives are discussed in Sect. 4.

2 A Novel Denoising Method for Medical CT Images

The proposed method is to combine Shearlet and BM3D with a moving decomposition framework (MDF). With MDF, the image will be decomposed into two components. One component will contain details and texture of the image whereas the other component will be similar to the original image only with the gradient's norm subtracted. These two components contain different information allowing different parts of image to be dealt with in different ways.

2.1 Moving Decomposition Framework

This section introduces the moving decomposition framework (MDF) [9]. Let $I : \Gamma \subset R^2 \rightarrow R$ be a gray-level image, and (x, y) be the standard coordinate system of R^2. I_x and I_y denote the derivatives of I with respect to x and y respectively. ∂I denotes the gradient of I. The decomposition is divided into two stages. In the first stage, an orthonormal moving frame P was constructed by I_x, I_y and ∂I. In the second stage, the components $(J1, J2, J3)$ of the R^3-valued function were computed in that moving

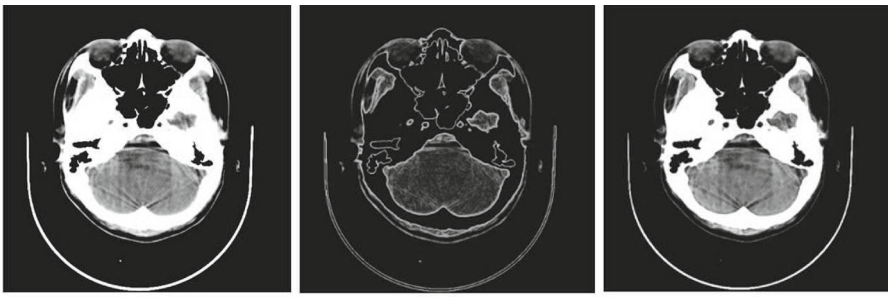

Fig. 1 Set $\mu = 0.05$, **a** original CT image, **b** $J1$ component obtained by moving frame decomposition, **c** $J3$ component obtained by moving frame decomposition

frame. The moving frame P is defined as follows:

$$\mathbf{P(x,y)} = \begin{pmatrix} \frac{I_x(x,y)}{\sqrt{|\partial I(x,y)|^2(1+\mu^2|\partial I(x,y)|^2)}} & \frac{-I_y(x,y)}{|\partial I(x,y)|} & \frac{-\mu I_x(x,y)}{\sqrt{(1+\mu^2|\partial I(x,y)|^2)}} \\ \frac{I_y(x,y)}{\sqrt{|\partial I(x,y)|^2(1+\mu^2|\partial I(x,y)|^2)}} & \frac{I_x(x,y)}{|\partial I(x,y)|} & \frac{-\mu I_y(x,y)}{\sqrt{(1+\mu^2|\partial I(x,y)|^2)}} \\ \frac{\mu|\partial I(x,y)|^2}{\sqrt{|\partial I(x,y)|^2(1+\mu^2|\partial I(x,y)|^2)}} & 0 & \frac{1}{\sqrt{(1+\mu^2|\partial I(x,y)|^2)}} \end{pmatrix} \tag{1}$$

It should be noted μ is a scale parameter and its value has an obvious influence on denoising performance. The results of denoising the image after applying the decomposition frame are the same as the results of denoising the image directly for $\lim \mu \to 0$. The higher the value of μ, the better the recovery of the clean component $J3$, whereas the smaller the value of μ, the better the recovery of the clean component $J1$. Components $(J1, J2, J3)$ of each pixel are computed as follows:

$$\begin{pmatrix} J1(x,y) \\ J2(x,y) \\ J3(x,y) \end{pmatrix} = P^{-1}(x,y) \begin{pmatrix} 0 \\ 0 \\ I(x,y) \end{pmatrix} \tag{2}$$

In Fig. 1, component $J1$ contains the edges and textures of the image whereas component $J3$ is similar to the original image.

$$\begin{pmatrix} \delta(x,y) \\ \tau(x,y) \\ \hat{I}(x,y) \end{pmatrix} = P(x,y) \begin{pmatrix} \mathrm{Jrec1}(x,y) \\ J2(x,y) \\ \mathrm{Jrec3}(x,y) \end{pmatrix} \tag{3}$$

where Jrec1 and Jrec3 denote the denoised version of $J1$ and $J3$ respectively, and $\hat{I}(x,y)$ is the pixel of denoised image. The decomposition framework enables the gradient information and approximate information of the image to be processed separately and efficiently.

2.2 Shearlet Transformation and Its Discretization

Since being introduced in 2005, the Shearlet system became the distinctive approach capable of deal with multiple dimension signals [12]. Shearlets have the advantages of simple mathematical structure, multi-resolution, multi-directionality and localization. Nowadays, Shearlets have been widely used in the domain of signal processing, in areas such as image denoising, image fusion, edge detection, etc.

The Shearlet system is defined as follows:

$$SH(\Omega) = \left\{ \Omega_{a,s,t} := a^{-\frac{3}{4}} \Omega(A_a^{-1} S_s^{-1} \cdot (-t)) : a \in R^*, s \in R, t \in R^2 \right\} \tag{4}$$

where A, S are $n \times n$ invertible matrices and $|\det S| = 1$. A, S are defined as follows:

$$A = \begin{pmatrix} a & 0 \\ 0 & \sqrt{a} \end{pmatrix} \qquad S = \begin{pmatrix} 1 & -s \\ 0 & 1 \end{pmatrix}$$

Discrete data processing must be used when the algorithm is implemented and the image is processed. In order to make the framework of continuous Shearlet transformation applicable to data processing, it is necessary to discretize the continuous Shearlet. Discrete Shearlet is actually obtained by discretizing the parameters of continuous Shearlet under certain conditions. In this paper, we discretized the Shearlet system using band-limited Shearlets. We chose band-limited Shearlets because it does allow a high localization in frequency domain and it does admit a precise digitization of the continuum theory which is important for image denoising. Better localization means that we can use different algorithms to deal with the corresponding regions more effectively, and more accurate digitization enables us, to a greater extent, to reduce the loss of image information caused by discretization, and the results of image processing will be closer to ideal situation.

In order to provide support for the inverse transformation of the Shearlet, the Shearlet system must conform to the Parseval frame defined as follows:

$$\sum_{j,l,k} \left| \langle f, \varphi_{j,l,k} \rangle \right|^2 = \|f\|^2 \tag{5}$$

Set $\hat{\varphi}(\xi)$ be the Fourier transformation of $\varphi_{j,l,k}$, for any $\xi = (\xi_1, \xi_2) \in \hat{R}^2$, $\xi_1 \neq 0$. Let $\varphi_{j,l,k}$ satisfy:

$$\hat{\varphi}(\xi) = \hat{\varphi}(\xi_1, \xi_2) = \hat{\varphi}_1(\xi_1) \hat{\varphi}_2 \left(\frac{\xi_2}{\xi_1} \right) \tag{6}$$

where $\hat{\varphi}_1, \hat{\varphi}_2 \in C^\infty\left(\hat{R}\right)$, supp $\hat{\varphi}_1 \subset \left[-\frac{1}{2}, -\frac{1}{16}\right] \cup \left[\frac{1}{16}, \frac{1}{2}\right]$ and supp $\hat{\varphi}_2 \subset [-1, 1]$, and thus the frequency support of $\hat{\varphi}(\xi)$ can be obtained:

$$\hat{\varphi}_{j,l,k} \subset \begin{pmatrix} (\xi_1, \xi_2) : \xi_1 \in \left[-2^{2j-1}, -2^{2j-4}\right] \cup \left[2^{2j-4}, 2^{2j-1}\right] \\ \left| \frac{\xi_1}{\xi_2} + l 2^{-j} \right| \leq 2^{-j} \end{pmatrix} \tag{7}$$

The discretized Shear matrix becomes A_{2^j} and the parabolic scale matrix becomes S_k in formula (5). After discretization, the function parameter (a, s, t) in formula (4) changes into

$(2^{-j}, -k2^{-\frac{j}{2}}, A_{2^j}^{-1} S_k^{-1}\,\mathrm{cm}), c \in (R_+)^2$. Set $c = (c_1, c_2) \in (R_+)^2$, the discrete Shearlet system in Fourier domain is as follow:

$$\begin{aligned}\hat{\psi}_{j,k,m}(\omega) &= \hat{\psi}(A_{a_j}^T S_{s_{j,k}}^T \omega) e^{-2\pi i \langle \omega, t_m \rangle} \\ &= \hat{\psi}_1(4^{-j}\omega_1)\hat{\psi}_2(2^j \frac{\omega_2}{\omega_1} + k) e^{-2\pi i \langle \omega, \frac{m_1}{M} \frac{m_2}{N} \rangle}, \omega \in \Omega \end{aligned} \tag{8}$$

$$\Omega(\omega_1, \omega_2) := \begin{pmatrix} \omega_1 = -\left\lfloor \frac{M}{2} \right\rfloor, \ldots, \left\lceil \frac{M}{2} \right\rceil - 1 \\ \omega_2 = -\left\lfloor \frac{N}{2} \right\rfloor, \ldots, \left\lceil \frac{N}{2} \right\rceil - 1 \end{pmatrix} \tag{9}$$

When the parameters meet $a \leq 1$ and $|s| \leq 1$, the segmentation caused by the cone boundary will occur at $|k| = 2^j$, only in the situation of $|s| = 1$. For these two cones, it can be seen that two half Shearlets at $|s| = 1$ have a gap at the joint. The gap in these conical regions is the undefined region of Shearlet. In order to fill these gaps to obtain the frequency domain support of the complete Shearlet, we glue the three parts together by superposition. The formulas of discrete Shearlet transformation are as follows:

$$\mathrm{SH}(f)(\eta, j, m, k) := \begin{pmatrix} \langle f, \varphi_m \rangle, \eta = 0 \\ \left\langle f, \psi_{j,k,m}^{\eta} \right\rangle, \eta \in \{h, v\} \\ \left\langle f, \psi_{j,k,m}^{h \times v} \right\rangle, \eta = \times, |k| = 2^j \end{pmatrix} \tag{10}$$

where $j = 0, 1, \ldots, j_0 - 1$, and $1 - 2^j \leq |k| \leq 2^j - 1$.

2.3 Process of Shearlet Transformation-Based Denoising

This section introduces the process of Shearlet transformation-based denoising. Let I denote the image, L is the number of layers the image will be decomposed into, and j is the number of layers the image is currently decomposing. Main steps of the Shearlet transformation are:

- Pyramid filters will be applied to image I to obtain high-pass band image $I_{\mathrm{high}}\, j$ and low-pass band image $I_{\mathrm{low}}\, j$.
- Converting $I_{\mathrm{high}}\, j$ into pseudo-polar coordinates by Fourier transformation, and then obtain $P_{\mathrm{Ihigh}}\, j$ which is in pseudo-polar coordinates.
- Applying direction bandpass filter to $P_{\mathrm{Ihigh}}\, j$.
- Applying two dimensional inverse FFT or inverse pseudo-polar discrete Fourier transformation (PDFT) to $P_{\mathrm{Ihigh}}\, j$ to obtain corresponding Shearlet coefficients.
- Set $j = j + 1$, and repeat the previous steps until $j = L$.

2.4 Block Matching 3D Denoising (BM3D)

Block Matching 3D denoising (BM3D) uses the redundant information of an image to perform denoising [5, 14]. There is a connection between adjacent pixels in an image. BM3D takes advantage of this connection. It groups similar blocks, establishes a 3D array, and converts the 3D array into a sparse representation in the transform domain by using the collaborative filtering method to restore the image. The combination of transform domain method and grouping technique enables BM3D to obtain an excellent sparse representation of group data. BM3D thus has the ability to obtain great PSNR values of denoised image whilst also preserving some essential unique features of the image.

The BM3D algorithm includes two key steps and is presented as follows:

1. **Step one:**
   - Searching the neighborhood of each block in the image, finding similar blocks and stacking these blocks to form a 3D array. All similar blocks of reference blocks form a set of 3D arrays.
   - Converting these 3D arrays into transform domain, and conducting collaborative filtering to the coefficients by hard thresholding. Applying the inverse transform to these coefficients to obtain the estimation for each block.
   - Computing the basic estimate of the true-image by weighted averaging all of the obtained block-wise estimates that overlap.
2. **Step two:**
   - Grouping the basic estimate of the true-image as in step one, finding the similar blocks in the basic estimate of the true-image, using the same location of these blocks to obtain another group in the noisy image.
   - Applying the Wiener filter to both groups to obtain a second estimate. Using the energy spectrum of the basic estimate as the true energy spectrum when performing the Wiener filter to the group of noisy image.
   - Using a weighted average to compute a final estimate of the true-image as at the end of step one.

However, BM3D also has its shortcomings. Its high complexity means that BM3D cannot be processed in real time and the literature [26] points out nonlocal similarity might not be fully exploited. In fact, it is possible that image details of similar blocks may be weakened or blurred by the BM3D algorithm, particularly under the circumstance of strong noise. In the method proposed in this paper, BM3D will be applied to deal with the noisy version of component J3, obtained by applying a decomposition frame to the noisy image, to avoid blurring the detail of the real image.

2.5 Steps of the Proposed Denoising Method for Medical CT Images

Different from general image denoising, medical image denoising requires preserving more details, because some initial lesions may appear in the details of the image. Therefore, for medical CT image denoising, it is more suitable to use different denoising

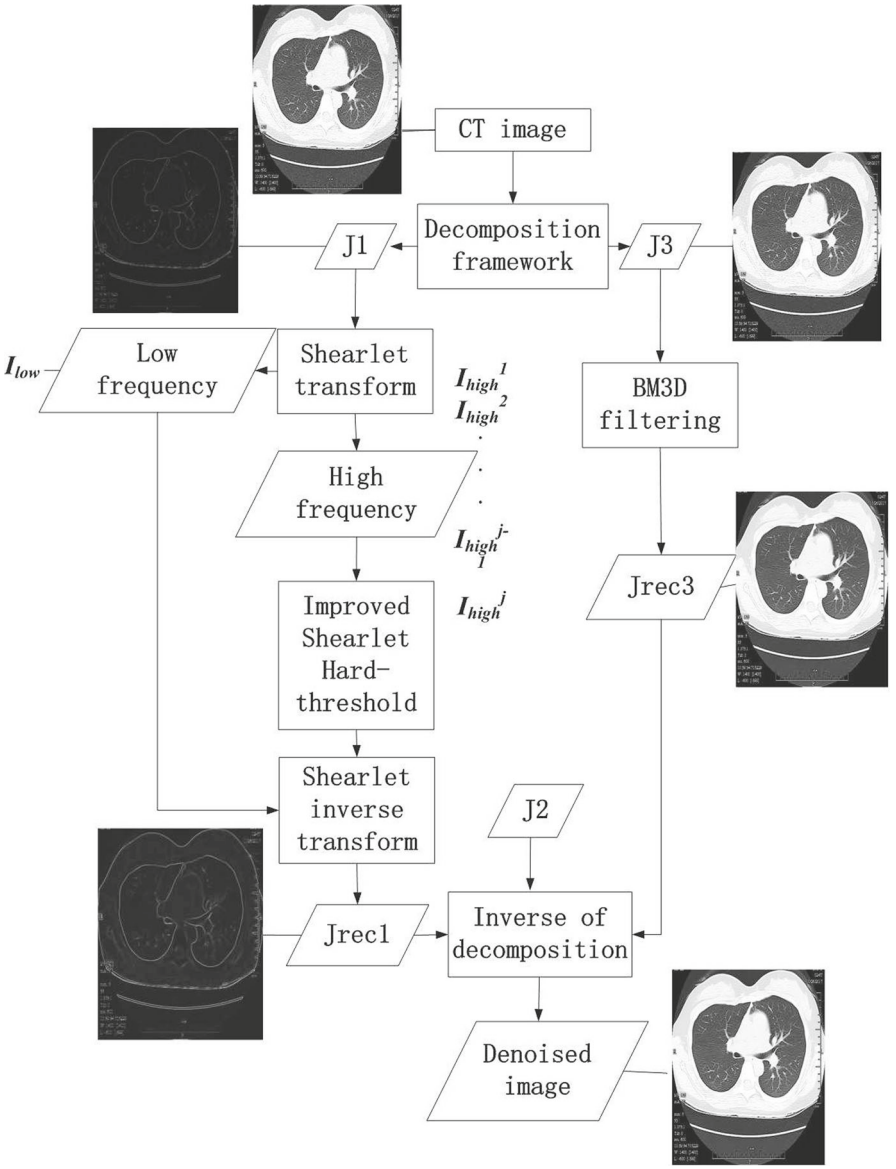

Fig. 2 The schematic diagram of the proposed framework and integrated approach

methods to deal with the high frequency band and low frequency band respectively. The proposed method takes this characteristic into account by using MDF to decompose CT image and deals with components respectively. The proposed denoising approach is described in algorithm 1, and the schematic diagram and main steps of the proposed framework and approach are shown in Fig. 2.

Algorithm 1: The Proposed Denoising Method for Medical CT Images

Input:

- Observed CT image $I \in R^{N\times N}$
- Patch size $p \in R^{M\times M}$

Output:

- The estimation of noiseless CT image $\hat{I} \in R^{N\times N}$

Procedure:

- Construct a decomposition frame P
- $J1, J2(Zero), J3 \leftarrow P^{-1}(x,y)\begin{pmatrix} 0 \\ 0 \\ I(x,y) \end{pmatrix}$
- $J1^1_{high}, \cdots, J1^j_{high} \overset{ST}{\Longleftarrow} J1$
- $Jrec1^1_{high}, \cdots, Jrec1^j_{high} \overset{ThresholdingShrinkage}{\Longleftarrow} J1^n_{high}, (n = 1, \cdots, j)$
- $Jrec1 \overset{IST}{\Longleftarrow} Jrec1^1_{high}, \cdots, Jrec1^j_{high}$
- $Jrec3 \overset{BM3D}{\Longleftarrow} J3$
- $\hat{I} \leftarrow P(x,y)\begin{pmatrix} Jrec1(x,y) \\ J2(x,y) \\ Jrec3(x,y) \end{pmatrix}$

In the above algorithmic steps, ST denotes Shearlet Transformation and IST denotes Inverse Shearlet transformation. $J1$, $J2$ and $J3$ are the three components generated by MDF decomposition.

Remark 1 After MDF decomposition, component J2 is actually a zero matrix which contains only zero elements. Components $J1$ and $J3$ need to be processed in the following denoising steps with Shearlet Transformation-based denoising method and BM3D denoising respectively, while component $J2$ (zero matrix) requires no additional processing.

Different from general image denoising, medical image denoising must reduce the image noise while retaining the image details. Firstly, based on the moving decomposition framework (MDF), the proposed method encodes the image pixel by pixel with a small-size sliding window box, and decomposes the details (mainly high frequency) and non-details (the approximate components, mainly low frequency) parts from the original noisy image. For these two parts, Shearlet-based denoising and the block matching and 3D filtering (BM3D) denoising are applied respectively. The multi-directionality and multi-scale property of the Shearlet make it possible to obtain better effect in denoising the detail parts, and the BM3D denoising algorithm can also obtain ideal denoising results in denoising the approximate components (mainly low frequency part) of the image. Finally, with the two processed components and the inverse transformation method of the decomposition frame, the denoised image is obtained.

The original noisy CT image is decomposed by decomposition frame and then processed separately, so that the details and edges of the CT image can be better preserved. The final denoising results obtained by this proposed integrated method not only ensure the effect of image denoising, but also retain CT image details and edges well. It is confirmed with simulation and clinical experiments that the final denoising results, obtained by denoising the details and non-details parts with their corresponding methods after MDF decomposition, will be better than the results obtained by using the algorithm directly for the medical image.

3 Experimental Studies of the Proposed Denoising Method

Experimental studies of the proposed denoising approach are presented in this section. Studies were conducted on two simulated CT images and on two clinical CT images with various degrees of noise variance respectively and their denoising performances are provided. Comparative studies of the proposed method against other existing denoising algorithms are also presented. The algorithms chosen for comparison were BM3D [5], Shearlet [10], NLM [2], and K-SVD [1]. The software used in the experiments was MATLAB R2014a. In simulation study, the GWNoisy2 function was used to simulate noise to the image within the parameters of noise intensity. Each algorithm window measures $5 * 5$. The 'thresh' function in ShearLab-1.1 was used to conduct threshold processing in the process of Shearlet-based denoising.

Assuming the noise variance of image is N, and the parameter 'sigma' in Shearlet shrinkage denoising will be selected as $a * N$. In the process of BM3D, the parameter 'sigma' in function BM3D will be selected as $b * N$. The values of a and b were obtained through the experiments. These showed the $J1$ component will be very weak when μ is selected as 0.0001. In order not to destroy the edge details in the $J1$ component when denoising, the threshold is very small.

Through simulations and experiments, the parameters were chosen as following: $a = \frac{1}{25}$, for $\mu = 0.001$ and $a = \frac{1}{87}$, for $\mu = 0.0001$. $b = 1.02$.

3.1 Evaluating Indices

(1) Peak Signal-to-Noise Ratio (PSNR)

In the evaluation of denoising performance, peak signal to noise ratio (PSNR) is adopted as a comparison indicator to conduct a quantitative analysis. The formula for PSNR is as follows:

$$\mathrm{PSNR}\left(I, \bar{I}\right) = 10\log_{10}\left(\frac{255^2}{\mathrm{MSE}}\right) \tag{11}$$

where $\bar{I}$ denotes the denoised image, and I the original image.

The expression of MSE is:

$$\mathrm{MSE} = \frac{1}{MN}\sum_{i=1}^{M}\sum_{j=1}^{N}\left(I_{i,j} - \bar{I}_{i,j}\right)^2 \tag{12}$$

where M and N are the length and width of the two-dimensional code respectively. The larger the MSE value, the worse the image quality.

(2) Structural Similarity (SSIM)

SSIM is used to measure the structure similarity of two images, and its formula is defined as follows:

$$\mathrm{SSIM}(I, \bar{I}) = l(I, \bar{I})c(I, \bar{I})s(I, \bar{I}) \tag{13}$$

where $l(I, \bar{I}) = \frac{2\mu_I\mu_{\bar{I}}+C_1}{\mu_I^2+\mu_{\bar{I}}^2+C_2}$ is used to measure the average brightness similarity of two images. μ_I, $\mu_{\bar{I}}$ and σ_I^2, $\sigma_{\bar{I}}^2$ represent the mean and variance of the noise-free reference image and the estimated image respectively. $c(I, \bar{I}) = \frac{2\sigma_I\sigma_{\bar{I}}+C_2}{\sigma_I^2+\sigma_{\bar{I}}^2+C_2}$ is a function that reflects the similarity of two images. $s(I, \bar{I}) = \frac{\sigma_{I,\bar{I}}+C_3}{\sigma_I\sigma_{\bar{I}}+C_3}$ is the correlation coefficient function between the measured images, and $\sigma_{I,\bar{I}}$ represents the covariance between I and $\bar{I}$.

The SSIM value is in the range of [0 1], the higher the value of SSIM, the higher the similarity between I and $\bar{I}$. Variables C_1, C_2, C_3 are positive integer regularization parameters, and these variables are added to avoid denominator to be zero. $C_1 = (k_1L)^2$, $C_2 = (k_2L)^2$, $k_1 = 0.01, k_2 = 0.03$, L denotes max range of image pixel values, and $C_3 = 0.5C_2$

(3) Pratt's Figure of Merit (FoM)

FoM is utilized to numerically evaluate the quality of edge detectors and is defined as follows:

$$\mathrm{FoM}(I, \bar{I}) = \frac{1}{\max(P_I, P_{\bar{I}})}\sum_{i=0}^{P_I}\frac{1}{1+\alpha d_i^2} \tag{14}$$

where P_I and $P_{\bar{I}}$ represent the number of pixels that are ideal and actually detected edge of the image respectively. α is a constant which is usually taken $\alpha = 1/9$, and d_i represents the distance between the edge pixel and the nearest ideal edge pixel. The range of FoM is [0,1], and the higher the FoM value, the higher the coincidence degree. When FoM value is 1, this indicates the edge of the detected image is exactly the same as the ideal image edge.

3.2 Experimental Results on Simulated Images

Simulated CT1 and CT2 images for the denoising experimental studies are shown in Fig. 3. Tables 1 and 2 with different δ show the proposed approach has a better effect on simulated CT images denoising than other algorithms. As Fig. 4 shows, the texture of simulated CT1 image denoised with the proposed approach (Fig. 4b) has been preserved better than other algorithms while most of the noise has been removed. BM3D (Fig. 4c), Shearlet (Fig. 4d), K-svd (Fig. 4e) and NLM (Fig. 4f) blur the details of the original image in different degrees. This is particularly the case in Fig. 4f, the image denoised by NLM, for the blurring of the image means the details in the original image can hardly be seen. The comparison of denoising results of the proposed approach with other existing algorithms for simulated CT1 image is shown in Fig. 5. It can be seen, as noise variances increase, the advantages of the quantitative

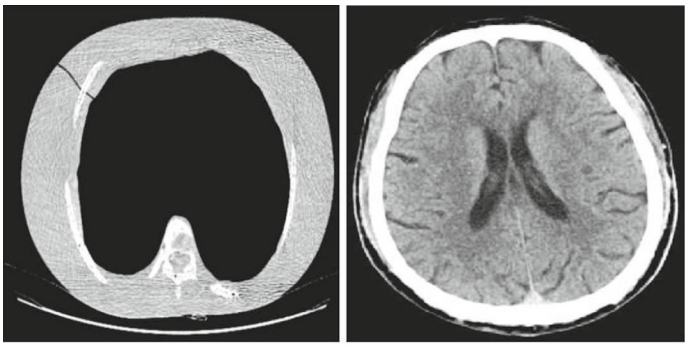

Fig. 3 **a** simulated CT1, **b** simulated CT2

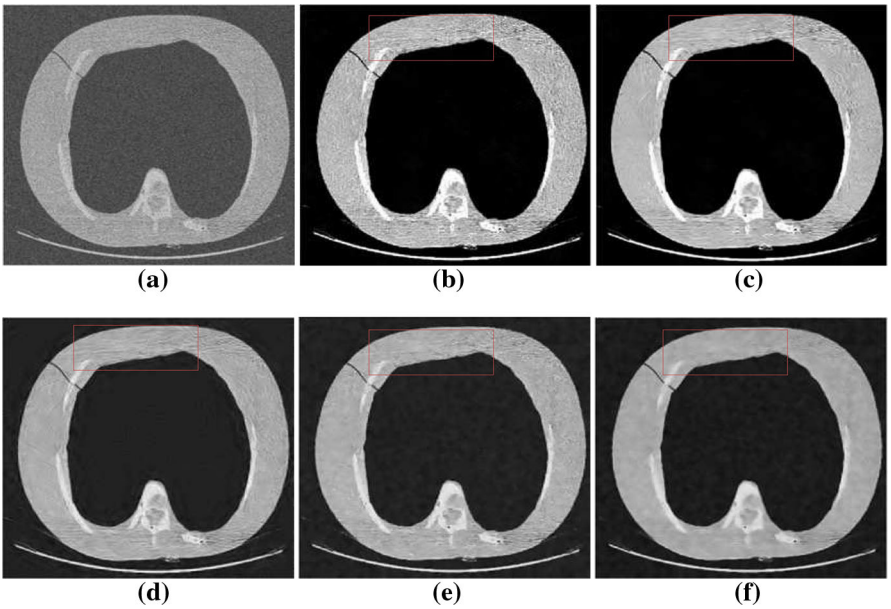

Fig. 4 $\mu = 0.001$ and $\delta = 40$, **a** the noisy simulated CT1 image , **b** denoised by proposed method, **c** by BM3D, **d** by Shearlet transform, **f** by K-svd, **g** by NLM

results obtained by the proposed method (blue line) over other methods also gradually increases. It is pretty clear the proposed method has the most effective denoising ability.

In most cases, the difference between CT images and ordinary images is that medical images have more detailed textures. This makes it more difficult to distinguish the noise from the real image. The ability of a denoising algorithm to preserve image texture structure is therefore particularly important in medical image denoising. The denoised version of simulated CT2 image is shown in Fig. 6. The performances of denoising the simulated CT2 image are shown in Table 2 and in Fig. 8 respectively.

Table 1 Comparison of denoising performances for simulated CT1 image

	Methods	Proposed $\mu = 0.0001$	Proposed $\mu = 0.001$	BM3D	Shearlet	K-svd	NLM
$\delta = 40$	PSNR	26.2150	26.2028	25.9913	24.9863	25.5241	24.5509
	SSIM	0.7615	0.7381	0.7166	0.6006	0.5588	0.4949
	FoM	0.8011	0.8344	0.8145	0.7560	0.7743	0.7304
$\delta = 30$	PSNR	27.6648	27.5858	27.3568	25.8814	26.9597	25.5497
	SSIM	0.8309	0.8211	0.8049	0.6795	0.6800	0.6029
	FoM	0.8554	0.8592	0.8488	0.8266	0.8043	0.7229
$\delta = 20$	PSNR	29.6620	29.6603	29.6492	27.5752	29.3274	27.7062
	SSIM	0.8946	0.8927	0.8946	0.7740	0.8026	0.7493
	FoM	0.8527	0.8606	0.8513	0.8459	0.8500	0.7944
$\delta = 10$	PSNR	34.2556	34.2241	34.2197	31.5244	33.9401	32.6923
	SSIM	0.9678	0.9664	0.9677	0.9003	0.9249	0.9243
	FoM	0.9209	0.9226	0.9192	0.9172	0.9284	0.9116

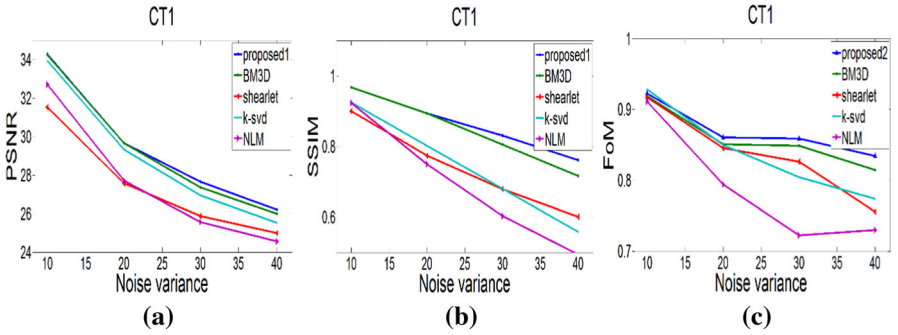

Fig. 5 Comparison of performances for denoising of the simulated CT1 images. **a** PSNR, **b** SSIM, **c** FoM

To show the image more intuitively, Fig. 7 presents two components before and after denoising process to show the relationship between the denoising of $J1$ and $J3$ components.

As can be seen from Fig. 7, the denoised $J1$ component (c) has lost most of its texture but preserved its edges information, and the denoised $J3$ component (d) is similar to its original image. Actually, the performances of different evaluation indices of resulting denoised images are relative to those of $J1$ and $J2$ components.

Figure 6 shows the proposed method (Fig. 6b) has filtered almost all noise in the noisy image, and blurred some details and edges in origin image while filtering. The results of Shearlet (Fig. 6d), K-svd (Fig. 6e) and NLM (Fig. 6f) are not satisfactory. The results of Shearlet (Fig. 6d) add too much scratch in the denoised image not present in the original image. The results of K-svd (Fig. 6e) and NLM (Fig. 6f) have corrupted a large amount of structural information in the original figure. The results of BM3D (Fig. 6c) seem to have better edge preservation than the proposed method (Fig. 6b), but as can be seen from Fig. 8, the proposed method has better performances than those of

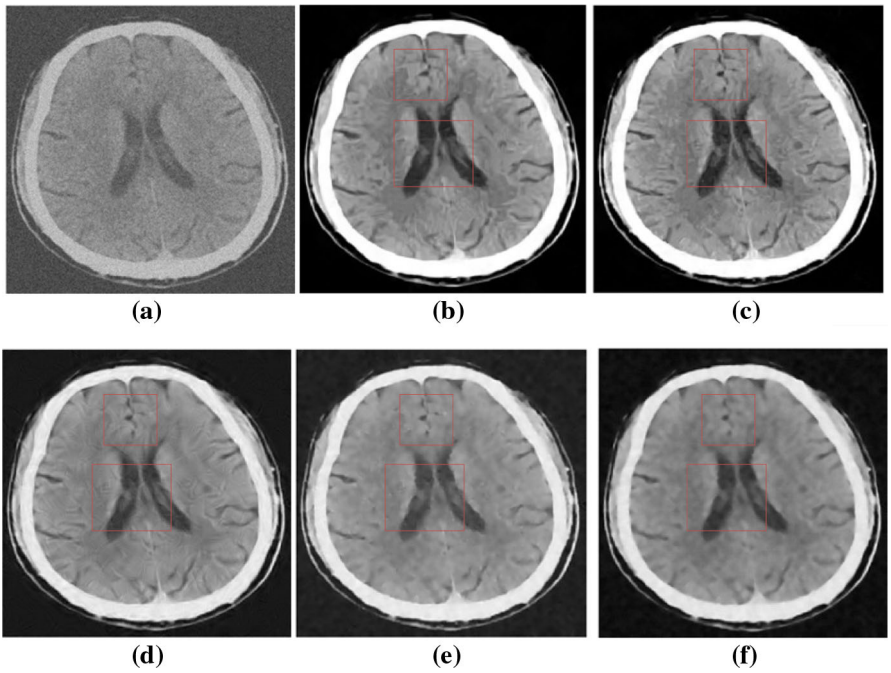

Fig. 6 $\mu = 0.001$ and $\delta = 40$, **a** the noisy simulated CT2 image, **b** denoised by proposed method, **c** by BM3D, **d** by Shearlet transformation, **f** by K-svd, **g** by NLM

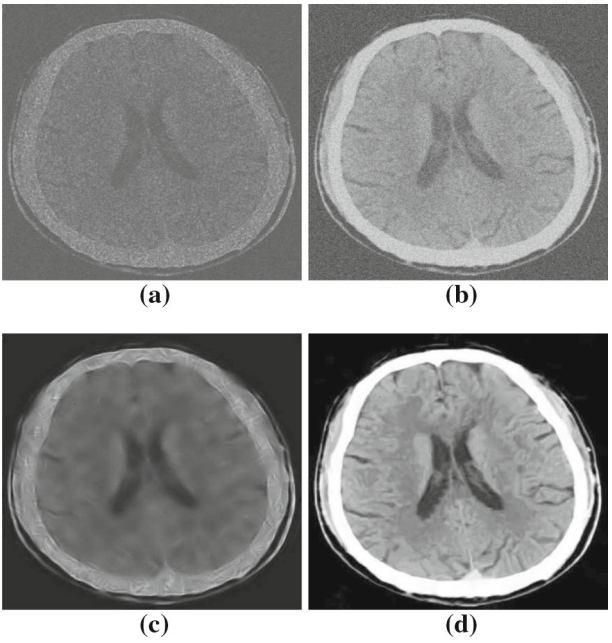

Fig. 7 **a** $J1$ noisy image, **b** $J3$ noisy image, **c** denoised $J1$ image, **d** denoised $J3$ image

Table 2 Comparison of denoising performances for simulated CT2 image

	Methods	Proposed $\mu = 0.0001$	Proposed $\mu = 0.001$	BM3D	Shearlet	K-svd	NLM
$\delta = 40$	PSNR	30.3395	30.2441	30.0706	29.3294	29.1359	28.2858
	SSIM	0.7965	0.7962	0.7839	0.7337	0.6894	0.6546
	FoM	0.8394	0.8411	0.7981	0.8016	0.7503	0.7145
$\delta = 30$	PSNR	31.5219	31.5008	31.4580	30.6223	30.4096	29.3252
	SSIM	0.8278	0.8104	0.8262	0.7815	0.7370	0.6029
	FoM	0.8413	0.8550	0.8229	0.8302	0.7498	0.7229
$\delta = 20$	PSNR	33.4165	33.4425	33.4083	32.5099	32.4511	31.1015
	SSIM	0.8850	0.8840	0.8835	0.8432	0.8174	0.7493
	FoM	0.8883	0.8828	0.8833	0.8911	0.8750	0.7944
$\delta = 10$	PSNR	37.1157	37.1306	37.1231	36.0385	36.5804	34.1641
	SSIM	0.9454	0.9477	0.9468	0.9229	0.9257	0.8797
	FoM	0.9245	0.9366	0.9203	0.9111	0.9027	0.9213

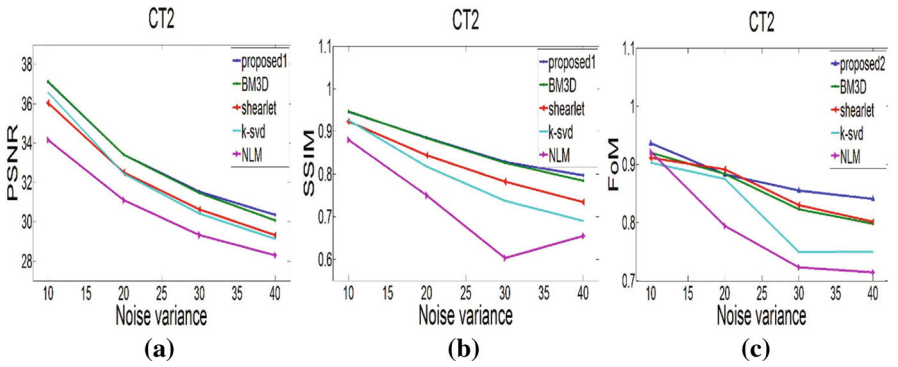

Fig. 8 Comparison of performances for denoising of simulated CT2 images. **a** PSNR, **b** SSIM, **c** FoM

other algorithms. The PSNR, SSIM and FoM of the denoised image obtained by the proposed method have advantages over those by other algorithms. As a result of these experiments, in most cases the proposed algorithm was found to have advantages over the others. The proposed method can obtain a better performance than that of BM3D or Shearlet alone. The denoised images obtained by the proposed method not only have a higher PSNR, but also remove image noise whilst simultaneously preserving the edge of the images. This is reflected in the fact that the proposed algorithm can achieve higher SSIM and FoM. The selection of μ depends on the characteristics of the image. For general cases, the restoration of medical images focuses more on the structure of the restored images, and thus in the case of serious noise disturbance, a value of μ is suggested as 0.0001.

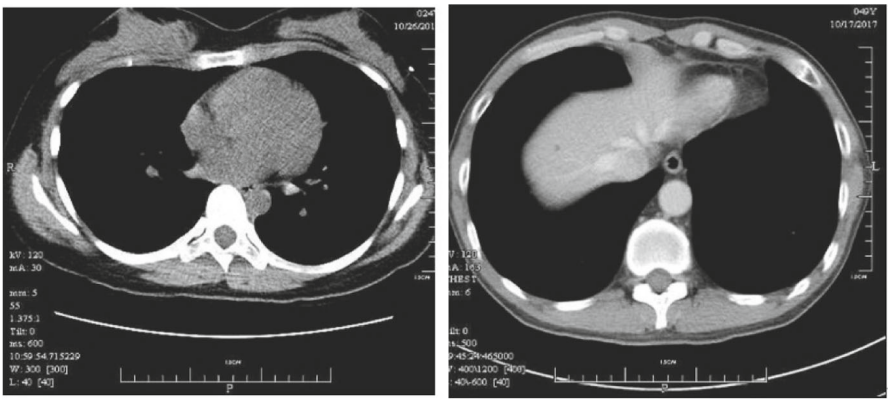

(a) (b)

Fig. 9 **a** Mediastina window, **b** Pulmonary window

Table 3 Comparison of denoising results for real CT1 image and real CT2 image

Methods	Noisy image	Proposed	BM3D	Shearlet	K-svd	NLM
NIQE(CT1)	5.5240	8.7373	8.5066	6.2396	6.7275	8.4316
NIQE(CT2)	5.1950	10.9593	10.8352	7.2465	8.4867	10.0697

3.3 Experimental Results on Real Clinical CT Images

This section presents experimental results on two real clinical CT images. The experiments are conducted on a pulmonary window CT image and on a mediastina window CT image respectively. The resolutions of CT images are $512 * 512$ and 256 gray scales. Two clinical CT images are shown in Fig. 9.

Because a noise-free real CT image does not exist, the natural image quality evaluator (NIQE) which is a completely blind image quality analyzer has been applied to evaluate the quality of an image.

It is obvious that the proposed method, as shown in Figs. 10a and 11a, can effectively remove noise and simultaneously preserve the details of clinical CT images. BM3D is similarly effective as shown in Figs. 10b and 11b. Nevertheless, as can be seen in Table 3, the NIQE values of the proposed method is best, meaning it obtains better results compared to BM3D filtering. The CT images smoothened by Shearlet as seen in Figs. 10c and 11c, have some striped interference like cracks in the filtered CT images. The images filtered by K-svd shown in Fig. 10d and 11d, show some improvements on noise suppressing, but do not perform as well as expected. The NLM, shown in Figs. 10e and 11e, have good performances in suppressing the noise but at the cost of obscuring the edge of the CT images.

Remark 2 In the field of image denoising, such as some medical images, sparse representation still plays an important role. The K-SVD method realizes denoising by sparse coding. The discrete Fourier transform or wavelet transform, for example, yields a

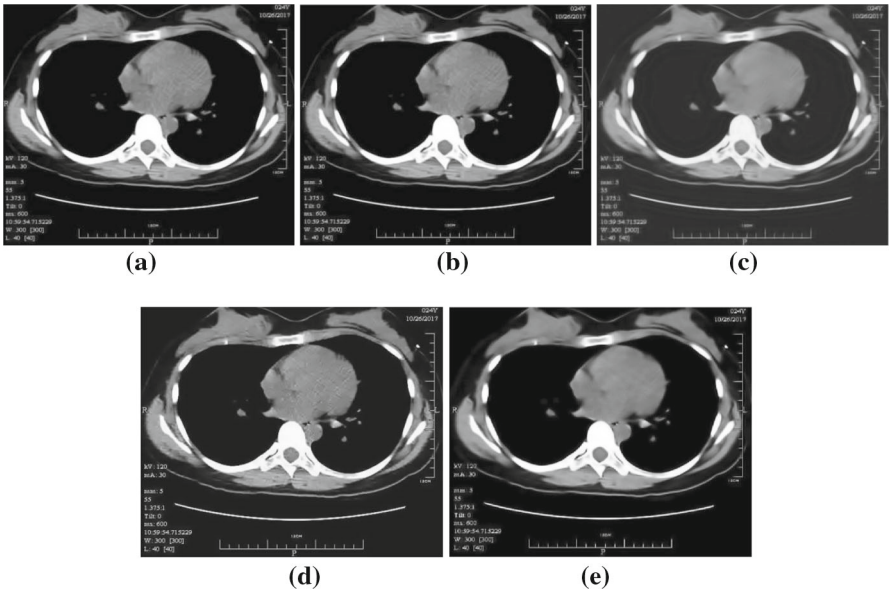

Fig. 10 Denoised results of clinical CT1 images. **a** by proposed method, **b** by BM3D, **c** by Shearlet, **d** by K-svd, **e** by NLM

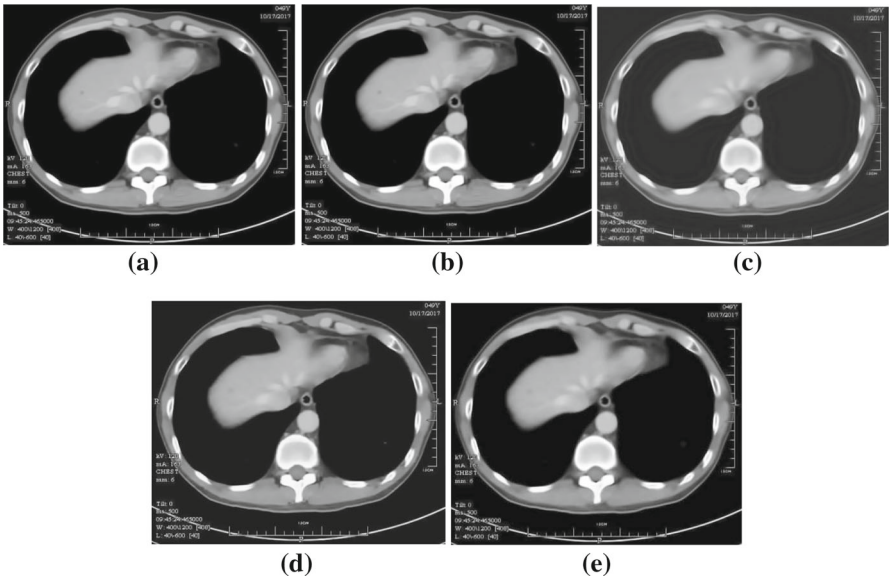

Fig. 11 Denoised results of clinical CT2 images. **a** by proposed method, **b** by BM3D, **c** by Shearlet, **d** by K-svd, **e** by NLM

series of orthogonal bases, while the dictionary obtained by sparse representation is a series of non-orthogonal bases. An orthogonal basis can only represent a certain feature of an image, but not other features at the same time. Therefore, the sparsity of an orthogonal basis is not as good as that of a non-orthogonal basis. However, medical CT images are more monotonous than natural images, and their attributes are too simple. As a result, more noise components are learned as atoms for its dictionary learning, and thus K-SVD has a worse performance for denoising of CT images.

Remark 3 It is true that the denoising performance improvements shown in the last few sections of the paper are likely to extend to a wider class of medical images, for instance, to ultrasound medical images. According to the existing literature, in the transform domain, the distribution of speckle noise in the clinical ultrasound image is, to some extent, similar to that in the Low Dose CT images, and thus the improvements are likely to extend to ultrasound medical images.

Remark 4 Recently, we also carried out research on CT image denoising method based on deep learning. Based on multi-feature extraction and convolutional neural network, we proposed a method for CT image denoising, and compared its performance with that of BM3D, KSCV, DnCNN, and FFDNet [25]. According to the research results, denoising methods based on deep learning have better denoising performances than that of BM3D, KSVD and other denoising methods. Meanwhile, the deep learning-based denoising methods also have slightly better performances than that of the method established in this paper. However, because of black box nature of deep learning-based method, difficulty of obtaining the corresponding dataset with enough labeled CT images, problem of the generalization ability of the trained model, dependence on neural network structure model and training data set, a large number of network parameter calculations and updates in the training process, and the low training efficiency of the network, deep learning-based denoising methods usually make it difficult to obtain stable results in CT image denoising.

4 Conclusions

This paper proposes a novel integrated denoising algorithm that combines BM3D and Shearlet in a moving decomposition framework (MDF). Simulations and clinical experiments were conducted and comparisons with other existing methods made. The results show the proposed denoising method can obtain better performances in terms of PSNR value, SSIM and FoM. From experimental studies, it can be seen in terms of the evaluation index FoM, that the proposed algorithm has a better ability to retain edges when the value of μ is selected at 0.001. By experiment, it was determined that the value of μ is related to the effectiveness of the denoising of the two components after decomposition on the final denoising image. The value of μ is proportional to the contribution of the denoising effectiveness of $J1$ component on the final denoising image, and inversely proportional to $J3$. The optimal selection of the value of μ remains an open problem requiring further research. For the selection of parameters a and b of the threshold function, optimal selection depends on image characteristics

and the hardware environment in which the experiments are conducted, and these also need further study.

Acknowledgements This work is partially supported by the National Natural Science Foundation of China (60974042).

Data Availability We confirm that the data is available upon reasonable request.

References

1. M. Aharon, M. Elad, A. Bruckstein, K-SVD: an algorithm for designing overcomplete dictionaries for sparse representation. IEEE Trans. Signal Process. **54**(11), 4311–4322 (2006)
2. A. Buades, B. Coll, J.M. Morel, A Non-Local Algorithm for Image Denoising, Computer Vision and Pattern Recognition. CVPR 2005. IEEE Computer Society Conference (2005)
3. M. Chen, Y.F. Pu, Y.C. Bai, A fractional-order variational residual CNN for low dose CT Image denoising, in *Intelligent Computing Theories and Application. ICIC 2019. Lecture Notes in Computer Science*, vol. 11643, ed. by D.S. Huang, V. Bevilacqua, P. Premaratne (Springer, Cham, 2019)
4. Y. Chen, X. Yin, L. Shi et al., Improving abdomen tumor low-dose CT images using a fast dictionary learning based processing. Phys. Med. Biol. **58**(16), 5803–5820 (2013)
5. K. Dabov, A. Foi, V. Katkovnik, K. Egiazarian, Image denoising by sparse 3-D transform-domain collaborative filtering. IEEE Trans. Image Process. **16**(8), 2080–2095 (2007)
6. Z. Dan, X. Chen, H. Gan, C. Gao, Locally Adaptive Shearlet Denoising Based on Bayesian MAP Estimate. in Sixth International Conference on Image and Graphics (IEEE Computer Society, HeFeihina, 2011)
7. M. Diwakar, M. Kumar, A review on CT image noise and its denoising. Biomed. Signal Process. Control **42**(1), 73–88 (2018)
8. M. Diwakar, M. Kumar, CT image denoising using NLM and correlation-based wavelet packet thresholding. IEEE Image Process. **12**(5), 708–715 (2018)
9. G. Ghimpeteanu, T. Batard, M. Bertalmío, S. Levine, A decomposition framework for image denoising algorithms. IEEE Trans. Image Process. **25**(1), 388–399 (2016)
10. K. Guo, D. Labate, Optimally sparse multidimensional representation using shearlets. SIAM J. Math. Anal. **39**(1), 298–318 (2007)
11. M. Kumar, M. Diwakar, A new exponentially directional weighted function based CT image denoising using total variation. J. King Saud Univ. Comput. Inf. Sci. (2016). https://doi.org/10.1016/j.jksuci.2016.12.002
12. G. Kutyniok, D. Labate et al., *Shearlets: Multiscale Analysis for Multivariate Data* (Birkhäuser, Boston, 2012)
13. G. Kutyniok, W. Lim, G. Steidl, Shearlets: theory and applications. GAMM- Mitteilungen **37**(2), 259–280 (2014)
14. Y.J. Li, J. Zhang, M. Wang, Improved BM3D denoising method. IET Image Proc. **11**(12), 1197–1204 (2017)
15. Z. Li, L. Yu, J.D. Trzasko et al., Adaptive nonlocal means filtering based on local noise level for CT denoising. Med. Phys. **41**(1), 011908 (2014)
16. J. Ma, J. Huang, Q. Feng et al., Low-dose computed tomography image restoration using previous normal-dose scan. Med. Phys. **38**(10), 5713–5731 (2011)
17. S. Mallat, *A Wavelet Tour of Signal Processing* (Academic Press, San Diego, 1998)
18. C. McLeavy, M. Chunara, R. Gravell, A. Rauf, A. Cushnie, C.S. Talbot et al., The future of CT: deep learning reconstruction. Clin. Radiol. **76**, 407–15 (2021)
19. J. Mohan, V. Krishnaveni, Y. Guo, A survey on the magnetic resonance image denoising methods. Biomed. Signal Process. Control **9**(1), 56–69 (2014)
20. C.W. Tian, Y. Xua, Z.Y. Li, W. Zuo, L. Fei, H. Liu, Attention-guided CNN for image denoising. Neural Netw. **124**, 117–129 (2020)
21. Q. Yang, P. Yan, Y. Zhang et al., Low dose CT image denoising using a generative adversarial network with Wasserstein distance and perceptual loss. IEEE Trans. Med. Imaging **37**(6), 1348–1357 (2018)

22. S. Yi, D. Labate, G.R. Easley, H. Krim, A Shearlet approach to edge analysis and detection. IEEE Trans. Image Process. **18**(5), 929–941 (2009)
23. K. Zhang, W. Zuo, Y. Chen, D. Meng, L. Zhang, Beyond a Gaussian denoiser: residual learning of deep CNN for image denoising. IEEE Trans. Image Process. **26**, 3142–55 (2017)
24. K. Zhang, W. Zuo, L. Zhang, FFDNet: toward a fast and flexible solution for CNN-based image denoising. IEEE Trans. Image Process. **27**, 4608–22 (2018)
25. J. Zhang, H.L. Zhou, Y. Niu, J.C. Lv, J. Chen, Y. Cheng, CNN and multi-feature extraction based denoising of medical CT images. Biomed. Signal Process. Control **67**, 102545 (2021)
26. H. Zhong, K. Ma, Y. Zhou, Modified BM3D algorithm for image denoising using nonlocal centralization prior. Signal Process. **106**(2), 342–347 (2015)